HHS Public Access

Author manuscript

Ann Neurol. Author manuscript; available in PMC 2022 December 01.

Published in final edited form as:

Ann Neurol. 2021 December ; 90(6): 913–926. doi:10.1002/ana.26235.

Impact of Cardiopulmonary Bypass on Neurogenesis and Cortical Maturation

Zaenab Dhari, MD[1,*], **Camille Leonetti, PhD**[1,*], **Stephen Lin, MEngr**[2], **Arianna Prince, BS**[1,3], **James Howick, MD, MS**[1], **David Zurakowski, MS, PhD**[4], **Paul C. Wang, PhD**[2,5], **Richard A. Jonas, MD**[1,3], **Nobuyuki Ishibashi, MD**[1,3]

[1]Children's National Heart Institute, Center for Neuroscience Research, Sheikh Zayed Institute for Pediatric Surgical Innovation, Children's National Hospital, Washington, DC

[2]Department of Radiology, Howard University, Washington, DC

[3]George Washington University School of Medicine and Health Science, Washington, DC

[4]Department of Anesthesiology, Critical Care and Pain Medicine Research, Boston Children's Hospital, Boston, MA

[5]Department of Electrical Engineering, Fu Jen Catholic University, New Taipei City, Taiwan

Abstract

Objective: Neurodevelopmental delays and frontal lobe cortical dysmaturation are widespread among children with congenital heart disease (CHD). The subventricular zone (SVZ) is the largest pool of neural stem/progenitor cells in the postnatal brain. Our aim is to determine the effects of cardiopulmonary bypass (CPB) on neurogenesis and cortical maturation in piglets whose SVZ development is similar to human infants.

Methods: Three week-old piglets (n=29) were randomly assigned to control (no surgery), mild-CPB (34°C full flow for 60min) and severe-CPB groups (25°C circulatory-arrest for 60min). The SVZ and frontal lobe were analyzed with immunohistochemistry 3 days and 4 weeks postoperatively. MRI of the frontal lobe was used to assess cortical development.

Results: SVZ neurogenic activity was reduced up to 4 weeks after both mild and severe CPB-induced insults. CPB also induced decreased migration of young neurons to the frontal lobe, demonstrating that CPB impairs postnatal neurogenesis. MRI 4 weeks after CPB displayed a decrease in gyrification index and cortical volume of the frontal lobe. Cortical fractional anisotropy was increased after severe CPB injury, indicating a prolonged deleterious impact of CPB on cortical maturation. Both CPB-induced insults displayed a significant change in densities

Corresponding author: Nobuyuki Ishibashi, MD, Children's National Hospital, 111 Michigan Avenue, NW, M7640, Washington, DC 20010. Telephone number: 202-476-2388, Fax number: 202-476-2388, nishibas@childrensnational.org.

*equally contributed authors

Author contributions

For this manuscript, C.L. and N.I. were responsible for study concept and design. Z.D., C.L., S.L., A.P., J.H., D.Z., and P.C.W. contributed to data acquisition and analysis. Z.D. and C.L. drafted the manuscript and figures with R.A.J. and N.I. Z.D. and C.L. share the first author position. The authorship order among co–first authors was decided by volume of data acquisition used in the manuscript. All authors reviewed the manuscript before submission.

Potential Conflicts of Interest

Nothing to report.

of three major inhibitory neurons, suggesting excitatory-inhibitory imbalance in the frontal cortex. In addition, different CPB insults altered different subpopulations of inhibitory neurons.

Interpretation: Our results provide novel insights into cellular mechanisms contributing to CHD-induced neurological impairments. Further refinement of CPB hardware and techniques is necessary to improve long-term frontal cortical dysmaturation observed in children with CHD.

Introduction

Children with complex congenital heart diseases (CHD) are at risk of developing a wide spectrum of neurobehavioral problems[1,2]. Neuroimaging studies have shown that altered cortical morphology particularly affecting the frontal lobe, including reduced folding and volume, is present in children with severe and complex CHD[3,4]. Many of these changes are similar to the reductions in both cortical gray and white matter volume seen in children born prematurely[5]. Studies using diffusion tensor imaging (DTI) have demonstrated a high incidence of white matter dysmaturation and injury in CHD patients, including adolescents who underwent surgery in infancy[6,7].

Considerable previous work including our own has focused on the mechanisms of abnormal white matter development observed in the individual with CHD[8]. Exposure to the inflammatory effects of cardiopulmonary bypass (CPB) and possible hypoxia/ischemia associated with surgical repair in early infancy has been documented to interfere with white matter development[8–11]. The generation, migration, and maturation of oligodendrocytes responsible for myelin/white matter synthesis may be delayed by hypoxia due to CHD in the fetus[12,13].

Oligodendrocytes are glial cells generated by the subventricular zone (SVZ) particularly during the third trimester of human pregnancy and the first two or three years of life. However, in addition to generating glial cells responsible for white matter development, the SVZ is a key source of neurons generated from neuronal stem precursor cells (NSPCs). Furthermore young neurons in the SVZ migrate postnatally along the lateral ventricles to populate cortical gray matter, contributing to its further maturation[14]. Using a piglet model of fetal and neonatal hypoxia, we have previously documented reduced proliferation and neurogenesis in the SVZ accompanied by reduced cortical growth. We showed a similar reduction in neuroblasts within the SVZ of human infants born with CHD[15].

In the current study we examine the impact of cardiopulmonary bypass on neurogenic activity of the SVZ as well as growth and maturation of the frontal lobes.

Methods

Animals:

A total of 49 Yorkshire pigs were studied. CPB results in SIRS due to various factors including the repeated passage of blood through non-endothelial surfaces[16]. In addition, CHD patients are at risk of global cerebral ischemia during CPB resulting from a steal of blood by aorto-pulmonary collateral vessels and/or co-existing cerebral vessel abnormalities[17,18]. Emboli from solid particles or gaseous origin due to CPB are also

an important cause of ischemia/reperfusion (I/R) injury[17]. Finally, the circulatory arrest technique involves risk of I/R-injury such as the "no-reflow phenomenon"[19]. To investigate the effects of CPB on postnatal neurogenesis in the SVZ and frontal lobe development, CPB-induced brain insults were designed for this study to be primarily a result of SIRS alone or both SIRS and I/R-injury (Fig. 1A). A total of 29 female piglets at 3 weeks of age were randomly assigned to one of 3 groups with different CPB-induced brain insults that involved I/R injury and SIRS (1) No surgery (control, no insult, n=9); (2) 34°C full-flow bypass for 60min (mild-CPB insult, CPB-induced SIRS, n=10); and (3) 25°C hypothermic circulatory arrest (HCA) for 60min (severe-CPB insult, CPB-induced SIRS with I/R injury, n=10) (Fig. 1A). Animals were euthanized at either day 3 (n=12) or week 4 (n=17) post CPB to determine time-related changes in postnatal SVZ neurogenesis and frontal lobe development after cardiac surgery. Heterologous blood was obtained from a donor pig (n=20). We performed all experiments in compliance with the National Institutes of Health's "Guide for the Care and Use of Laboratory Animals" and the study was approved by the Animal Care and Use Committee at Children's National Hospital.

Juvenile Porcine CPB Model:

A thoracotomy was performed, and an arterial cannula and a venous cannula were inserted after heparinization. Fresh whole blood from a donor pig was transfused into the CPB circuit. The pump prime included normal saline, methylprednisolone, furosemide, sodium bicarbonate and cephazolin. The animals were perfused for 10min at 37°C and then cooled to 25°C or 34°C (Table 1). After cooling, HCA or maintenance of full flow was chosen (Table 1). After 40min of rewarming, animals were weaned from CPB. The hematocrit was maintained at 30% and pH-stat strategy was applied (Table 1)[17,20]. Blood pressure and temperature were monitored continuously. Arterial PO_2 and PCO_2, arterial pH, hematocrit value, and arterial lactate were measured. We used tissue oxygenation index (TOI) with Near-Infrared spectroscopy (NIRO-300) to assess cerebral ischemic status. Systemic leukocyte counts were performed to identify systemic inflammation. Neurological and behavioral evaluations were performed at 24hr intervals beginning on post-operative day 1. A total score of 400 indicates brain death while a score of 0 is considered normal. The score was accessed in a blinded fashion[9,10]. The details were described previously[8–10].

Cellular Assessment:

On post-operative day 3 or week 4 brains were resected and further post-fixed. Sections at 20μm thickness were incubated in primary and secondary antibodies as described previously[9,15]. The following antibodies were used for immunohistochemistry: anti-GFAP (1:1000;DAKO), Sox2 (1:500;Millipore), anti-ki67 (1:1000;BD Biosciences), anti-Doublecortin (1:1000;Millipore), anti-NeuN (1:500;Millipore), anti-Cleaved Caspase-3 (1:1000;Cell Signaling), anti-Calretinin (1:1000;Millipore), anti-Somatostatin (1:100;Millipore), anti-Parvalbumin (1:500;Millipore) and anti-Tbr1 (1:200;Abcam). Analysis of the SVZ was performed on coronal sections of the brain, adjacent to the wall of the lateral ventricles. We previously demonstrated that the anterior SVZ displays the most proliferating NSPCs and resembles its human counterpart[15]. Therefore we focused our analysis on the anterior SVZ (Fig. 1B–C). An imaginary line was drawn to divide the anterior SVZ into two regions: dorsolateral and ventral (Fig. 1D). The SVZ was

further subdivided into three tiers based on the density and distribution of DCX^+ cells as previously described in human brain[14]. All images were acquired with a Leica SP5 confocal laser-scanning microscope and counted in a blinded fashion. Given high cell density and homogeneous cell distribution, DCX^+ cell density was quantified by acquiring a total of 3 images for each region from separate microscopic fields at 40X magnification. For other stainings, the whole quantified area was scanned at 20X and tiled to avoid biased counting due to heterogeneous distribution in the large surface area. Regarding DCX^+ cluster analysis, only clusters with a surface larger than $140\mu m^2$ were counted in the analysis. The cluster occupancy was calculated by dividing the sum of all clusters surface area by the SVZ total surface area. The length of $GFAP^+$ processes lining the SVZ was perpendicularly measured every 50μm along the surface of the ventricle in a tile scan. For cellular analysis within the cortex, the following cortices were scanned separately based on the anatomical atlas and functional cortical map of the porcine brain: prefrontal cortex, somatosensory cortex, and insular cortex (Fig. 1E–F).

MRI and DTI:

We performed a total of 9 MRI studies (control; n=3, mild-CPB; n=3, severe-CPB; n=3) at week 4 after CPB (Fig. 1A). The images were transferred offline and reviewed by an MR physicist and a neuroradiologist. Conventional anatomical T1 and T2 MRI and diffusion tensor imaging (DTI) images were acquired on a GE Sigma HDxt 3.0T scanner. A minimum of 19 serial, coronal MRI images per piglet were analyzed for volumetric assessment and the gyrification index (GI)[15]. For DTI analysis: 9 serials of coronal images per piglet were used to analyze fractional anisotropy (FA) value in cortical grey matter. We applied a region-of-interest (ROI) approach to test specific structures through-out the brain selected. All ROIs were drawn and quantified manually by a blinded experimenter as we performed previously[8].

Statistics:

One-way analysis of variance (ANOVA) with Tukey's post-hoc comparisons was used to evaluate cellular and imaging outcome between the three treatment groups. Two-way ANOVA was used to look at CPB insult effects within SVZ and cortical regions, cortical layers, cell types or over time. Group-by-time and group-by-region interaction terms were evaluated in the ANOVA models. Statistical analysis was performed with PRISM software (GraphPad Software, Inc., La Jolla, CA). Significance was determined as two-tailed $P<0.05$ using Tukey post-hoc adjustment to control the experiment-wise error due to multiple comparisons[21]. Sample sizes of piglets for treatment and exposure groups provided 80% power to detect moderate to large effect sizes regarding neuronal cell measures at 3 days and 4 weeks post-surgery and group differences in cortical impairment[22]. All statistical analyses were reviewed by a biostatistics expert (D.Z.).

Results

Cardiopulmonary bypass alters neurogenesis in the piglet SVZ and disrupts neuroblast migrating chains toward the frontal lobe.

There were no differences among CPB groups in preoperative conditions (Tables 1 and 2). The TOI value during HCA was significantly lower than full-flow CPB (Table 1). The index was then normalized during the rewarming period (Table 1) demonstrating I/R injury in the severe-CPB insult (Fig. 1A). Lactate levels during cooling and at 3hrs post CPB were significantly higher in the severe-CPB group compared to the mild-CPB group (Table 1). Both mild- and severe-CPB insults caused a significant increase in leukocyte numbers 3hrs post CPB, but no difference was detected between the two CPB groups (Time $p<0.0001$, CPB $p=0.1413$) suggesting SIRS in the mild- and severe-CPB groups (Fig. 1A). Severe-CPB insult caused acute neurological symptoms, including seizures, whereas mild-CPB insult did not (Table 2). Neurological symptoms improved with time and were not present on postoperative day 7 (Table 2).

The SVZ retains its highly mitotic potential throughout postnatal life. We first examined the NSPC pool within the whole SVZ 3 days post-surgery. Although there were no differences in the density of $Sox2^+$ NSPCs at postoperative day 3 (control vs. mild $p=0.0605$, control vs. severe $p=0.0916$, mild vs. severe $p=0.9743$), detailed examination of the SVZ revealed a trend toward reduced NSPC proliferative capacity in the severe group compared to control (Fig. 2A–D). On the other hand, differences between CPB groups were not observed (Fig. 2D,E). There were no differences in the proliferative capacity between dorsolateral- and ventral-SVZ (Fig. 2E) as well as between analyzed tiers ($p=0.2198$), indicating no regional effects. Neurogenic activity was further assessed by quantifying the average length of $GFAP^+$ processes spanning tier 1 and expressed within radial-glia like cells (Fig. 2F–I). Both mild and severe groups displayed reduced $GFAP^+$ process length. This effect was confined to the dorsolateral part of the SVZ, as no differences were observed in the ventral part (Fig. 2J). These results are consistent with our previous studies showing that the dorsolateral SVZ is a more active neurogenic region than the ventral SVZ[15].

When we analyzed neuroblasts within the SVZ, decreased density of DCX^+ neuroblasts was observed in the peripheral region (tiers 2–3) in both mild and severe-CPB groups compared to control (Fig. 2K–O). While the effect of CPB on radial-glia like cells (i.e., neural stem cells) was restricted to the dorsolateral region (Fig. 2J), the density of neuroblasts was decreased in both dorsolateral and ventral parts of the SVZ after CPB (Fig. 2O). Although our previous studies found an unique role of HCA (i.e. severe-CPB insult) on developing white matter[9], we did not observe differences between mild and severe-CPB groups in NSPC proliferation, morphology of radial-glia like cells, or neuroblast density during the acute period after surgery. Together these data demonstrate that CPB alone can limit SVZ neurogenesis and reduce neuroblast density within the anterior dorsolateral-SVZ, the largest progenitor pool of the postnatal porcine brain.

A previous study in the human infant brain identified a chain-like structure of actively migrating DCX^+ neuroblasts with adherent junctions[14]. These chains principally located in the peripheral-SVZ (i.e., Tier 3) have been associated with a tangential migration oriented

toward the developing frontal cortex. To determine whether CPB-induced brain insults also alter neuroblast migratory chains, we analyzed DCX^+ clusters - coronal view of the migratory stream - within the SVZ (Fig. 2P–R). Although the average size of clusters was not different between the three groups tested, the number of clusters within the SVZ was reduced after severe-CPB insults (Fig. 2S). Our analysis also revealed that the overall occupancy of the clusters was significantly reduced in both mild and severe-CPB groups (Fig. 2T). In addition to reduction in SVZ neurogenesis, these data suggest that cardiac surgery during the early postnatal period alters neuroblast colonization into the frontal lobe of the neonatal and infant brain.

Cardiopulmonary bypass causes prolonged alterations in SVZ neurogenic properties and neuroblast migrating chains

To determine the long-term effects of cardiac surgery on SVZ neurogenic activity and the neuroblast population, we next examined the SVZ 4 weeks postoperatively. NSPC proliferation in the SVZ was significantly decreased for both mild- and severe-CPB groups (Fig. 3A–D). The extensive neurogenic activity of these regions has been described during the postnatal period[15]. Consistent with our previous findings, this prolonged decrease of proliferative capacity was specifically observed in the dorsolateral-SVZ (Fig. 3E). Our results also indicate that CPB insults significantly altered the number of $Sox2^+$ NSPCs ($p=0.0452$). Interestingly changes in NSPC proliferation from day 3 to week 4 significantly differed according to the type of CPB-induced insult (Fig. 3E). In the naïve SVZ, approximately 15% of NSPCs are able to maintain their proliferative capacity during this early postnatal period (Fig. 3E). In severe-CPB group, the proliferation of SVZ NSPCs was significantly inhibited as soon as 3 days after surgery and remained consistently low over time (Fig. 3E). On the other hand, we found that only 6% of $Sox2^+$ NSPCs on average can proliferate 4 weeks after CPB insult (Fig. 3E), indicating the critical role of systemic inflammation on the prolonged decline of proliferative ability after pediatric cardiac surgery. These observations were coupled to a marked reduction of $GFAP^+$ process length after both mild- and severe-CPB insults (Fig. 3F–I). Similar to the effects on NSPC proliferation, the impact of CPB on radial glia-like cells was especially deleterious in the dorsolateral-SVZ where $GFAP^+$ processes of radial glia-like cells remained shorter over time in both CPB groups compared to control (Fig. 3J). Altogether these results demonstrate the significant and prolonged deleterious impact of cardiac surgery on the largest NSPC pool in the neonatal and infant brain.

When we assessed the long-term effect of cardiac surgery on SVZ neuroblasts, reductions in cell density in the whole SVZ were displayed in both CPB groups (Fig. 3K–N). Consistent with our findings for NSPCs, the neuroblast population was reduced specifically in the dorsolateral-SVZ 4 weeks post CPB in both mild and severe insult groups (Fig. 3O), whereas no differences were observed in the ventral-SVZ (control vs. mild $p=0.1316$, control vs. severe $p=0.3868$, mild vs. severe $p=0.7261$). Moreover, similar to NSPCs, there was no recovery in neuroblast density over time (Fig. 3O), indicating prolonged inhibition of SVZ neurogenesis due to CPB. Finally, a marked reduction of cluster number and a trend in cluster occupancy was shown 4 weeks after severe-CPB (Fig. 3P–T). This latter observation specifically found in the group suggests a high susceptibility of migratory processes in

neuroblasts to HCA-induced injury (Fig. 1A). Overall, our cellular analysis of the SVZ up to 4 weeks post-operatively provides evidence that a CPB-induced insult not only reduces postnatal SVZ neurogenesis and neuroblast migration in the short-term, but also prevents recovery of the neurogenic properties of the largest progenitor pool for a prolonged period.

Cardiopulmonary bypass impairs cortical development and limits cortical expansion

Based on our previous finding that SVZ-derived cells populate the frontal cortex in neonatal piglets during normal development[15], we hypothesized that a reduction in the neuroblast number in the SVZ and structural alteration of neuroblast clusters could play an important role in cortical maturation after cardiac surgery. To test this hypothesis, we first assessed structural maturation of the developing cortex using a clinically-relevant neuroimaging approach 4 weeks after surgery. We did not observe any evidence of focal and/or multifocal injury post CPB. When the volumes of the entire frontal lobe and frontal cortex were quantified, however, both measurements in the mild and severe insult groups were significantly decreased compared to control (Fig. 4A–E). There were no differences in volumes between right and left hemispheres (total volume; p=0.7211, cortical volume; p=0.9887) indicating a global impact. Consistent with previous findings in gyrencephalic brain development[23,24], these observations were paired with a significant reduction in GI (Fig. 4F–I), demonstrating structural brain immaturity. Reduced cortical volume and impaired gyrification as observed in this animal model have been well documented in survivors after pediatric cardiac surgery[25]. Moreover, when we further compared DTI metrics between the three experimental groups, we found that animals exposed to a severe-CPB insult showed a significant increase in FA (Fig. 4J). FA values in the severe group were higher compared to mild-CPB FA values. As cortical microstructural maturation is associated with FA decrease[26], these observations indicate that CPB-induced systemic inflammation can cause aberrations in macrostructural cortical development, whereas HCA-induced injury during CPB induces microstructural changes.

To further understand the relationship between immature cortical development and depletion of neuroblasts in the SVZ, mature neuronal populations were analyzed within upper and lower layers of frontal cortices (Fig. 4K–M). We found that the density of $NeuN^+$ mature neurons varies between both cortical layers and experimental groups (Fig. 4O). Despite no statistical differences in the average density of neurons between the three groups (Fig. 4N), together with decreased cortical volume in the mild and severe groups (Fig. 4E) the results indicate an overall reduction in the total number of mature neurons in the frontal cortex after CPB.

Quantification of $Tbr1^+NeuN^+$ excitatory neurons showed a significant difference between layers as for $NeuN^+$ cells (Fig. 4O–T). Consistent with our previous findings[15], higher densities of excitatory neurons were found in the cortical lower layers compared to upper layers (Fig. 4T). On the other hand, no differences were observed in the density of excitatory neurons between CPB groups throughout the frontal lobe (Fig. 4P–T). Similarly, we did not observe differences in the densities of $NeuN^+$ mature neurons ($F=0.72$, $P=0.49$) and $Tbr1^+NeuN^+$ excitatory neurons ($F=0.89$, $P=0.43$) between prefrontal, somatosensory and insular cortices. Altogether our data demonstrate that CPB impairs cortical expansion and

microstructural maturation in an insult-dependent manner and limits the number of mature neurons in the frontal cortex of the infant brain.

Cardiopulmonary bypass alters specific subpopulations of interneurons in the frontal cortex

Given previous findings demonstrating that postnatal migrating neuroblasts differentiate into inhibitory neurons[14,15], we next examined the effects of CPB on GABAergic interneuron populations (i.e., inhibitory neurons) throughout the frontal cortex. Both experimental groups ($F=4.58$, $p=0.0224$) and distinguished cell types ($F=27.31$, $p<0.0001$) significantly affected the cell population 4 weeks post CPB. We found that CPB induced a significant change in the densities of three major GABAergic cell subpopulations: $CalR^+$, PV^+ and SST^+ interneurons (Fig. 5A–L, CPB: $P<0.05$). Moreover, a severe-CPB insult induced a significant decrease in densities of both PV^+ and SST^+ interneurons compared to control, specifically in lower cortical layers (Fig. 5E–L). There were no regional differences in the CPB-induced reduction of three interneuron populations ($CalR^+$ cells; $p=0.1709$, PV^+ cells; $p=0.0860$, SST^+ cells; $p=0.7555$). Notably, SST^+ interneuron density was also statistically lower in the severe insult group compared to the mild group (Fig. 5L). Together with our observations of an unchanged excitatory neuron population (Fig. 4S,T), this reduction of interneuron subpopulations 4 weeks after surgery indicates that CPB likely results in excitatory/inhibitory imbalance throughout the frontal cortex.

To assess whether the reduction in interneuron subpopulations was due to CPB-induced cell death or impaired integration of interneurons into the frontal cortex, we examined the effect of CPB on these cortical cell populations 3 days post-surgery. There was no difference in neuronal apoptosis, quantified as percentage of $Casp3^+NeuN^+$ apoptotic neurons per total $NeuN^+$ cells (Fig. 6D). Moreover, SST^+ and PV^+ cell densities were not affected 3 days after CPB (Fig. 6A–I), suggesting that cell apoptosis due to CPB is not a major underlying mechanism in the reduction of cortical interneurons observed following CPB. Since severe-CPB specifically decreases cluster number and occupancy in the SVZ for a prolonged period (Fig. 3P–T), our results suggest that HCA causes prolonged impairment in neuroblast migration from the SVZ and interferes with the integration of SST^+ and PV^+ interneurons into the frontal lobe, thereby causing microstructural alterations of the frontal cortex.

Discussion

This study is the first to reveal the impact of CPB on postnatal SVZ and cortical development in a porcine model which is anatomically and physiologically similar to humans. We demonstrated over a four-week recovery period that there are significant alterations of the NSPC pool and neuroblast populations in the SVZ resulting in a depletion of a source of interneurons destined to populate and potentially fine-tune development of the postnatal frontal cortex. Furthermore we noted decreased gyrencephaly and impairment of cortical expansion and maturation, which are pathological signatures observed commonly in survivors of neonatal cardiac surgery for complex CHD. Finally our study highlights CPB-induced excitatory/inhibitory imbalance throughout the frontal cortex and the distinct role of

CPB-induced I/R injury in cortical dysmaturation. Our findings provide new cellular insights into surgery-induced neonatal brain injury and guide us towards improving management of pediatric cardiac surgery to minimize neurological and behavioral consequences in the CHD population.

In the present study, the mild-CPB group was designed to determine the effects of common stressors in cardiac surgery including SIRS and oxidative stress, while the severe insult group allowed assessment of the additional impact of HCA-induced I/R injury. Our study demonstrated that both mild and severe-CPB insults induced early and late deleterious effects on the largest NSPC pool of postnatal brain and SVZ neurogenesis. It has been well documented previously that NSPCs are highly sensitive to inflammation[27,28] consistent with our finding of the impact of CPB-induced SIRS on neurogenesis in the neonatal brain. It is encouraging to note that stem cell proliferation can be restored by anti-inflammatory treatments[28].

The SVZ generates many neurons endogenously after birth[29]. It was recently found that neuroblasts continue to migrate postnatally along the lateral ventricles to populate the frontal lobe in the human infant, contributing to its further maturation[14]. We have previously demonstrated that reductions in NSPC proliferation and SVZ neurogenesis result in reduced cortical growth of the postnatal brain. We also showed that hypoxia affects $CalR^+$ interneurons and causes imbalance between excitatory and inhibitory neurons[15]. Consistent with these previous findings, our current data demonstrate reduced cortical folding (GI) and gray matter volume of the frontal lobe as well as excitatory/inhibitory imbalance after both mild- and severe-CPB insults indicating multifactorial etiology of impaired cortical maturation in children with CHD. Interestingly, reduction in these macrostructural MRI indices has been linked to delayed cognitive function[30,31]. Furthermore, excitatory/inhibitory imbalance in the prefrontal cortex has been strongly associated with intellectual and academic impairment[32]. Children with CHD frequently face delays in cognitive milestones that can be attributed to such imbalances[33,34]. In addition, changes in gamma oscillations, which are a product of the interplay between interneurons and excitatory principal cells[35], are commonly reported in psychiatric conditions[36,37]. To explore possible therapeutic approaches for improvement of cortical development in children with CHD, it will be important to define molecular targets that can prevent depletion of NSPC neurogenic potential and accelerate endogenous recovery through postnatal SVZ neurogenesis.

Our study demonstrates that I/R stress, only present in the severe group, is critical for the cortical dysmaturation of the frontal lobe determined by DTI. Similar with our findings, an increase in FA values is observed in the immature cortex of preterm children[38,39]. Current literature suggests that maturation of the neonatal cortex is associated with increased dendritic complexity which is correlated to decreased FA. Our detailed analysis of neuronal subpopulations revealed that severe-CPB decreases PV^+ and SST^+ interneuron populations. SST^+ interneurons influence other interneuron classes and also target the dendritic spines of pyramidal neurons. It has been demonstrated that this sub-population controls dendritic calcium spikes in pyramidal neurons, thus affecting learning tasks[40]. Fast-spiking PV^+ interneurons regulate local circuit dynamics[41], and PV^+ structural and physiological abnormalities have been strongly linked to psychiatric disorders[42]. Thus, a lack of these

inhibitory interneurons could provide some insight into the underlying mechanisms behind microstructural alterations such as reduced dendritic complexity observed after severe-CPB insults. Each interneuron subpopulation has a specific spatial origin and birthdate, and migrates during different developmental time windows[43]. In the present study, both mild and severe-CPB insults resulted in reduced cluster number and occupancy of neuroblast migratory chains on postoperative day 3, (i.e., 3 weeks of age) and affected the $CalR^+$ interneuron population. Similarly, in our previous study, chronic hypoxia from postnatal day 3 to 14 reduced $CalR^+$ interneurons[15]. On the other hand, we observed reduced migratory chains at 4 weeks post CPB (7 weeks of age) in the severe-CPB group together with decreases in PV^+ and SST^+ interneurons. The critical timing of damage in migrating neuroblasts may contribute to the distinct disruptions of this interneuron subpopulation that we noted between the mild and severe CPB groups.

We previously identified that the FA value from diffusion tensor imaging in the same piglet white matter structures at postnatal 3 weeks was equivalent to those of human post-conceptual 41–53 weeks[8]. On the other hand, GI of 7-week-old control piglet cortex in this study was approximately 1.5, which is similar to that of a human cortex at 37–38 week gestation in previous clinical studies. It is challenging to define the epochs in human cortical maturation that correspond to this piglet model because obvious technical/ethical difficulties prevent cellular investigations in the human brain during the late fetal and postnatal periods. However, our imaging studies indicate that the developmental time windows in the piglet model at this age correspond with the late gestation and early neonatal period in the human brain.

Higher mammals like pigs avoid many of the translational limitations encountered when studying rodents. The porcine brain has a gyrencephalic cortex and a multi-layered SVZ similar to the human SVZ[15]. The pig model has been widely used to investigate adverse effects of cardiac surgery and CPB[17,44]. Piglets undergoing CPB display white matter injury similar to that seen in human patients[8,9]. On the other hand, there are limitations in using juvenile pigs. Compared to studies with rodents, a small number of animals was assessed in each group. Although the deviation of physiological parameters in our studies were limited because of well-controlled procedure, it is possible that the small animal number caused the lack of difference between the mild and severe groups in NSPC proliferation, morphology of radial-glia like cells, or neuroblast density during the acute period after surgery. In addition, behavior tests used in this study showed that neurological deficits were resolved 1 day after mild-CPB and 7 days after severe-CPB injury, suggesting the limited sensitivity to assess long-term neurological impairments. Compared to rodents, region-specific neurobehavioral tests have not been well established in a porcine animal. Establishment of sophisticated behavior assays will be required for further improvement of this unique model. Our studies found increased cortical fractional anisotropy after severe CPB injury. However, the relationships between DTI signals and neuropathology in the cortex is more complex compared to white matter. For instance, previous studies indicated that the increased FA in the cortex following traumatic brain injury is associated with reactive astrocytes[45]. In addition, the presence of inflammation with microglia and macrophage activation significantly alters DTI indices[46]. More detailed analyses using the gyrencephalic piglet cortex will provide important data needed to better

interpret clinical human imaging studies. Our findings reflect the response of a normally developed brain to CPB because the animals used in this study did not experience fetal cerebral hypoxia. Therefore, it is possible that infants with complex CHD may experience these stresses differently based on their brain maturation status. Finally, in our studies two CPB injury groups were compared to naïve control, but not surgical control. Therefore, common surgery-induced insults such as anesthesia may affect some of our findings. Brain injury associated with pediatric cardiac surgery are multi-etiological. Although this study distinguished major CPB-induced insults between SIRS and I/R, future studies will be necessary to distinguish each factor individually from the global impact of cardiac surgery. On the other hand, our study provides a unique view of the roles of CPB and I/R on the largest NSPC niche and on cortical development.

In summary, our porcine model has given us insights into the cellular alterations that explain cortical dysmaturation occurring after CPB. Unraveling cellular/molecular events during surgery will enable us to design therapeutic approaches that can be restorative or reparative to the neurogenic potential of SVZ NSPCs and may reduce the undesirable impact of cardiac surgery. Further studies using this model will likely contribute to continuing refinement of pediatric cardiac surgery thereby improving the quality of life for children with complex CHD.

Acknowledgements

The authors would like to thank Drs. Ludmila Korotcova and Alexandru V. Korotcov for assistance for piglet surgeries and MRI scans. This work was supported by National Institutes of Health (NIH) grant R01HL139712 (N.I.) and R01HL146670 (N.I.) and by the Office of the Assistant Secretary of Defense for Health Affairs through the Peer Reviewed Medical Research Program under Award No. W81XWH2010199 (N.I.). This work was also supported by the District of Columbia Intellectual and Developmental Disabilities Research Center (DC-IDDRC) Award U54HD090257 by NICHD (PI: V. Gallo) and the NIH/NIMHHD U54MD007597 grant (PI: P.C. Wang). We are thankful for the vision and generosity of the Foglia and Hill families who also supported the cardiac surgery research laboratory.

References

1. Wernovsky G, Licht DJ. Neurodevelopmental Outcomes in Children With Congenital Heart Disease-What Can We Impact? Pediatr. Crit. Care Med 2016;17(8 Suppl 1):S232–42. [PubMed: 27490605]
2. Marelli A, Miller SP, Marino BS, et al. Brain in congenital heart disease across the lifespan: The cumulative burden of injury. Circulation 2016;133(20):1951–1962. [PubMed: 27185022]
3. Leonetti C, Back SA, Gallo V, Ishibashi N. Cortical Dysmaturation in Congenital Heart Disease. Trends Neurosci. 2019;42(3):192–204. [PubMed: 30616953]
4. Kelly CJ, Christiaens D, Batalle D, et al. Abnormal Microstructural Development of the Cerebral Cortex in Neonates With Congenital Heart Disease Is Associated With Impaired Cerebral Oxygen Delivery. J. Am. Heart Assoc 2019;8(5).
5. Counsell SJ, Boardman JP. Differential brain growth in the infant born preterm: Current knowledge and future developments from brain imaging. Semin. Fetal Neonatal Med 2005;10(5):403–410. [PubMed: 15993667]
6. Morton PD, Ishibashi N, Jonas RA, Gallo V. Congenital cardiac anomalies and white matter injury. Trends Neurosci. 2015;38(6):353–363. [PubMed: 25939892]
7. Miller SP, McQuillen PS, Hamrick S, et al. Abnormal Brain Development in Newborns with Congenital Heart Disease. N. Engl. J. Med 2007;357(19):1928–1938. [PubMed: 17989385]

8. Stinnett GR, Lin S, Korotcov AV., et al. Microstructural Alterations and Oligodendrocyte Dysmaturation in White Matter After Cardiopulmonary Bypass in a Juvenile Porcine Model. J. Am. Heart Assoc 2017;6(8)
9. Ishibashi N, Scafidi J, Murata A, et al. White matter protection in congenital heart surgery.. Circulation 2012;125(7):859–71. [PubMed: 22247493]
10. Korotcova L, Kumar S, Agematsu K, et al. Prolonged White Matter Inflammation After Cardiopulmonary Bypass and Circulatory Arrest in a Juvenile Porcine Model. Ann. Thorac. Surg 2015;100(3):1030–1037. [PubMed: 26228605]
11. Lynch JM, Buckley EM, Schwab PJ, et al. Time to surgery and preoperative cerebral hemodynamics predict postoperative white matter injury in neonates with hypoplastic left heart syndrome. J. Thorac. Cardiovasc. Surg 2014;148(5):2181–2188. [PubMed: 25109755]
12. Agematsu K, Korotcova L, Scafidi J, et al. Effects of preoperative hypoxia on white matter injury associated with cardiopulmonary bypass in a rodent hypoxic and brain slice model. Pediatr. Res 2014;75(5):618–625. [PubMed: 24488087]
13. Donofrio MT, Massaro AN. The impact of congenital heart disease on brain development and neurodevelopmental outcome. Int. J. Pediatr 2010;2010(359390):43–74.
14. Paredes MF, James D, Gil-Perotin S, et al. Extensive migration of young neurons into the infant human frontal lobe. Science 2016;354(6308):aaf7073. [PubMed: 27846470]
15. Morton PD, Korotcova L, Lewis BK, et al. Abnormal neurogenesis and cortical growth in congenital heart disease. Sci. Transl. Med 2017;9(374):eaah7029. [PubMed: 28123074]
16. Levy JH, Tanaka KA. Inflammatory response to cardiopulmonary bypass. Ann Thorac Surg. 2003;75:S715–20. [PubMed: 12607717]
17. Jonas RA. Deep hypothermic circulatory arrest: Current status and indications. Pediatr. Card. Surg. Annu 2002;5(1):76–88.
18. Schievink WI, Mokri B, Piepgras DG, Gittenberger-de Groot AC. Intracranial aneurysms and cervicocephalic arterial dissections associated with congenital heart disease. Neurosurgery 1996;39(4):685–690. [PubMed: 8880759]
19. Hickey PR. Endothelial and white cell activation in bypass and reperfusion injury: brain injury. Brain Inj. Pediatr. Card. Surg 1996;215–227.
20. Wypij D, Jonas RA, Bellinger DC, et al. The effect of hematocrit during hypothermic cardiopulmonary bypass in infant heart surgery: Results from the combined Boston hematocrit trials. J. Thorac. Cardiovasc. Surg 2008;135(2):355–360. [PubMed: 18242268]
21. Cabral HJ. Multiple comparisons procedures. Circulation 2008;117(5):698–701. [PubMed: 18250280]
22. Staffa SJ, Zurakowski D. Statistical power and sample size calculations: A primer for pediatric surgeons. J. Pediatr. Surg 2020;55(7):1173–1179. [PubMed: 31155391]
23. Li G, Wang L, Shi F, et al. Mapping longitudinal development of local cortical gyrification in infants from birth to 2 years of age. J. Neurosci 2014;34(12):4228–4238. [PubMed: 24647943]
24. Toro R, Perron M, Pike B, et al. Brain size and folding of the human cerebral cortex. Cereb. Cortex 2008;18(10):2352–2357. [PubMed: 18267953]
25. Claessens NHP, Moeskops P, Buchmann A, et al. Delayed cortical gray matter development in neonates with severe congenital heart disease. Pediatr. Res 2016;80(5):668–674. [PubMed: 27434120]
26. Ouyang M, Jeon T, Sotiras A, et al. Differential cortical microstructural maturation in the preterm human brain with diffusion kurtosis and tensor imaging. Proc. Natl. Acad. Sci. U. S. A 2019;116(10):4681–4688. [PubMed: 30782802]
27. Ekdahl CT, Claasen JH, Bonde S, et al. Inflammation is detrimental for neurogenesis in adult brain. Proc. Natl. Acad. Sci. U. S. A 2003;100(23):13632–13637. [PubMed: 14581618]
28. Gonzalez-Perez O, Gutierrez-Fernandez F, Lopez-Virgen V, et al. Immunological regulation of neurogenic niches in the adult brain. Neuroscience 2012;226:270–281. [PubMed: 22986164]
29. Sanai N, Nguyen T, Ihrie RA, et al. Corridors of migrating neurons in the human brain and their decline during infancy. Nature 2011;478(7369):382–6. [PubMed: 21964341]

30. Zhang Y, Zhou Y, Yu C, et al. Reduced cortical folding in mental retardation. Am. J. Neuroradiol 2010;31(6):1063–1067. [PubMed: 20075096]
31. Erus G, Battapady H, Satterthwaite TD, et al. Imaging patterns of brain development and their relationship to cognition. Cereb. Cortex 2015;25(6):1676–1684. [PubMed: 24421175]
32. Yizhar O, Fenno LE, Prigge M, et al. Neocortical excitation/inhibition balance in information processing and social dysfunction. Nature 2011;477(7363):171–178. [PubMed: 21796121]
33. Leonetti C, Back SA, Gallo V, Ishibashi N. Cortical Dysmaturation in Congenital Heart Disease. Trends Neurosci. 2019;42(3):192–204. [PubMed: 30616953]
34. Morton PD, Ishibashi N, Jonas RA. Neurodevelopmental Abnormalities and Congenital Heart Disease: Insights Into Altered Brain Maturation. Circ. Res 2017;120(6):960–977. [PubMed: 28302742]
35. Atallah BV, Scanziani M Instantaneous Modulation of Gamma Oscillation Frequency by Balancing Excitation with Inhibition. Neuron 2009;62(4):566–577. [PubMed: 19477157]
36. Fitzgerald PJ, Watson BO. Gamma oscillations as a biomarker for major depression: an emerging topic. Transl. Psychiatry 2018;8(1):177. [PubMed: 30181587]
37. Dienel SJ, Lewis DA. Alterations in cortical interneurons and cognitive function in schizophrenia. Neurobiol. Dis 2019;131.
38. DeIpolyi AR, Mukherjee P, Gill K, et al. Comparing microstructural and macrostructural development of the cerebral cortex in premature newborns: Diffusion tensor imaging versus cortical gyration. Neuroimage 2005;27(3):579–586. [PubMed: 15921934]
39. Neil JJ, Shiran SI, McKinstry RC, et al. Normal brain in human newborns: Apparent diffusion coefficient and diffusion anisotropy measured by using diffusion tensor MR imaging. Radiology 1998;209(1):57–66. [PubMed: 9769812]
40. Cichon J, Gan WB. Branch-specific dendritic Ca2+ spikes cause persistent synaptic plasticity. Nature 2015;520(7546):180–185. [PubMed: 25822789]
41. Ferguson BR, Gao WJ. Pv interneurons: critical regulators of E/I balance for prefrontal cortex-dependent behavior and psychiatric disorders. Front. Neural Circuits 2018;12:37. [PubMed: 29867371]
42. Marín O Interneuron dysfunction in psychiatric disorders. Nat. Rev. Neurosci 2012; 13(2):107–20. [PubMed: 22251963]
43. Lim L, Mi D, Llorca A, Marín O. Development and Functional Diversification of Cortical Interneurons. Neuron 2018;100(2):294–313. [PubMed: 30359598]
44. Ko TS, Mavroudis CD, Baker WB, et al. Non-invasive optical neuromonitoring of the temperature-dependence of cerebral oxygen metabolism during deep hypothermic cardiopulmonary bypass in neonatal swine. J. Cereb. Blood Flow Metab 2020;40(1):187–203. [PubMed: 30375917]
45. Budde MD, Janes L, Gold E, Turtzo LC and Frank JA. The contribution of gliosis to diffusion tensor anisotropy and tractography following traumatic brain injury: validation in the rat using Fourier analysis of stained tissue sections. Brain. 2011;134:2248–2260. [PubMed: 21764818]
46. Zhang J, Aggarwal M and Mori S. Structural insights into the rodent CNS via diffusion tensor imaging. Trends Neurosci. 2012;35:412–21. [PubMed: 22651954]

Summary for Social Media

1. If you and/or a co-author has a Twitter handle that you would like to be tagged, please enter it here. (format: @AUTHORSHANDLE). N/A
2. What is the current knowledge on the topic? Neurodevelopmental impairment is an important challenge for survivors after pediatric cardiac surgery with cardiopulmonary bypass. Neuroimaging studies have shown that altered cortical morphology particularly affecting the frontal lobe, including reduced folding and volume, is present in children with complex congenital heart diseases.
3. What question did this study address? The subventricular zone is the largest pool of neural stem and progenitor cells in the postnatal brain. We examined the impact of cardiopulmonary bypass on neurogenic activity of the subventricular zone as well as growth and maturation of the frontal lobes.
4. What does this study add to our knowledge? This study demonstrates the relationship between the subventricular zone and cortical growth after pediatric cardiac surgery and provides novel insights into cellular mechanisms contributing to neurological impairments in children with complex congenital heart disease.
5. How might this potentially impact on the practice of neurology? Our study indicates that treatments designed to protect and restore the neurogenic potential of neural stem and progenitor cells within the subventricular zone offer a promising avenue to prevent or reverse brain dysmaturation and to reduce neurological deficits in individuals with congenital heart disease

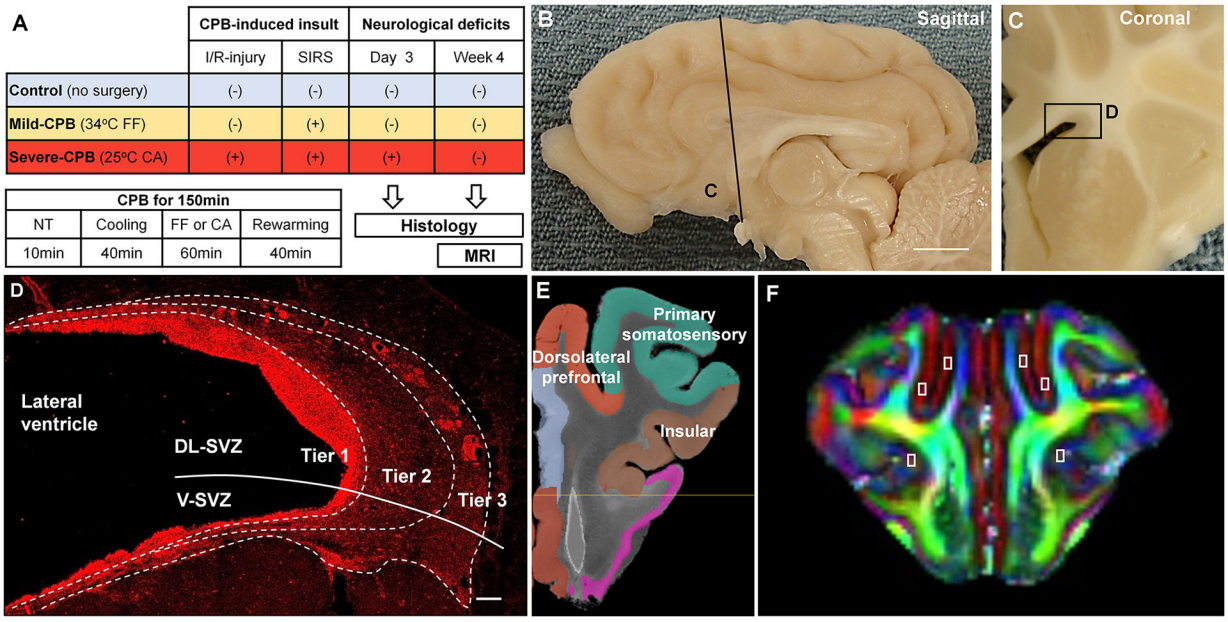

Figure 1. Methods.

(A) Overall study design. **(B)** Sagittal plane of the porcine brain. Scale bar, 1cm. **(C)** Coronal section and the SVZ (box D). **(D)** Magnified image from the boxed region in (**C**) and subdivision of the SVZ with doublecortin stain. Scale bar, 100 μm. **(E)** Anatomical location of cortical ROIs (Prefrontal, Primary Somatosensory, and Insular cortices). **(F)** DTI FA image of pig brain showing ROI of assessed cortical regions. CA, circulatory arrest; CPB, cardiopulmonary bypass; DL-SVZ, dorsolateral-SVZ; FF, full-flow perfusion; I/R, ischemia/reperfusion; NT, normothermia; SIRS, systemic inflammatory response syndrome; SVZ, subventricular zone; V-SVZ, ventral-SVZ.

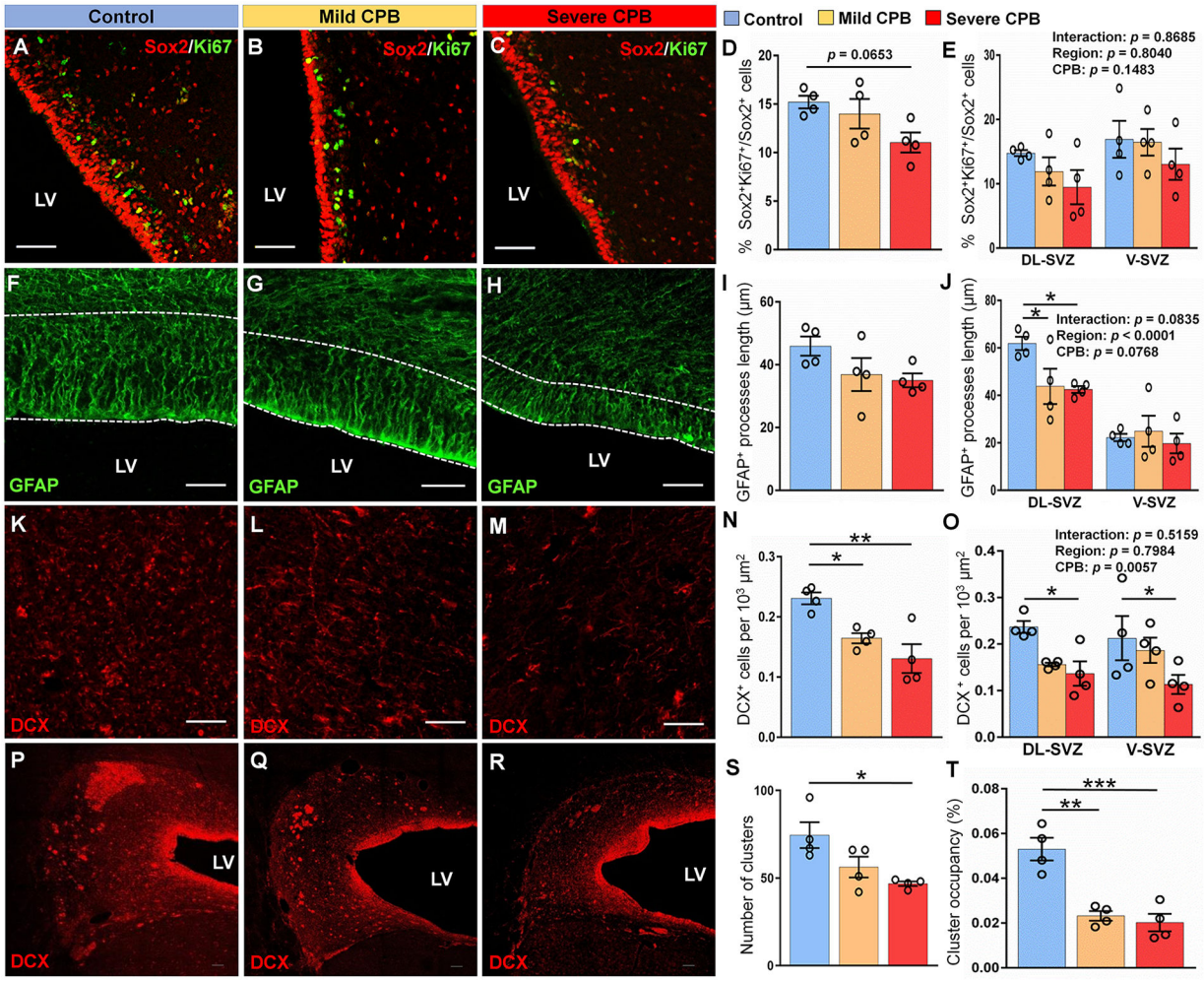

Figure 2. CPB impairs postnatal neurogenesis in the piglet SVZ 3 days post-surgery.

(A-C) Immunostains of $Sox2^{+}Ki67^{+}$ cells in the DL-SVZ. **(D, E)** Quantification of the percentage of proliferative $Sox2^{+}$ neural stem/progenitor cells. **(F-H)** Immunostains of GFAP in the DL-SVZ. **(I, J)** Quantification of the average length of $GFAP^{+}$ processes. **(K-M)** Immunostains of DCX^{+} cells in tiers 2–3 of the DL-SVZ. **(N, O)** Quantification of the average density of DCX^{+} cells. **(P-R)** Coronal sections of the SVZ showing immunostains of DCX^{+} cell clusters. **(S)** Quantification of the average number of DCX+ cell clusters. **(T)** Quantification of the average cluster occupancy of the SVZ. Scale bars, 50 µm (A, B, C, F, G, H, K, L, M) and 100 µm (P, Q, R). n = 4 animals per group. Data are expressed as mean ± SEM. $*p < 0.05$, $**p < 0.01$, $***p < 0.001$, one-way ANOVA with Tukey's post-hoc test (D, I, N, S, T) and two-way ANOVA with Tukey's post-hoc test (E, J, O). CPB, cardiopulmonary bypass; DL-SVZ, dorsolateral-SVZ; DCX, doublecortin; LV, lateral ventricle; SVZ, subventricular zone; V-SVZ, ventral-SVZ; GFAP, glial fibrillary acidic protein.

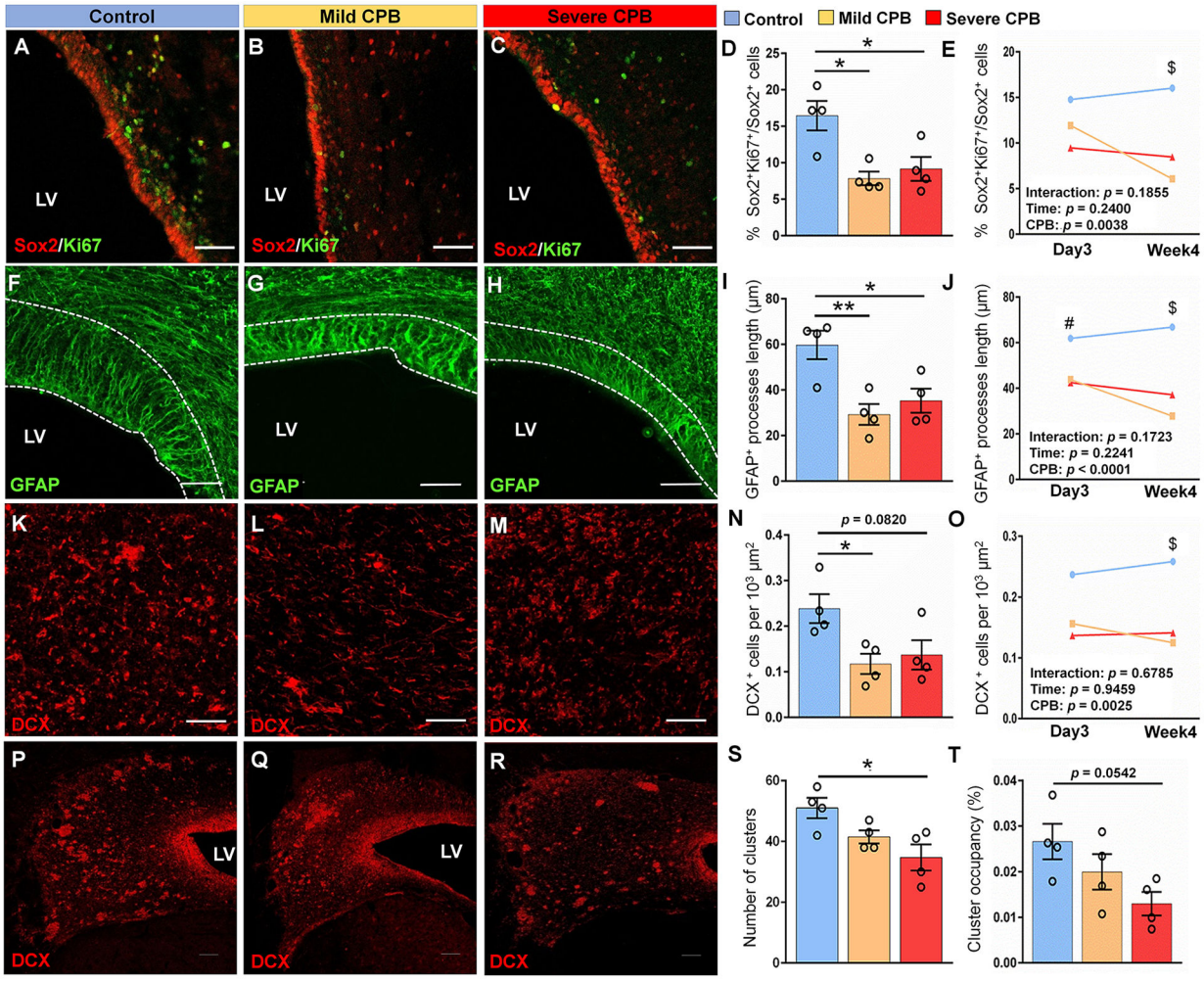

Figure 3. CPB causes a long-term disruption of SVZ neurogenesis 4 weeks post-surgery.

(A-C) Immunostains of $Sox2^{+}Ki67^{+}$ cells in the DL-SVZ. **(D)** Quantification of the percentage of proliferative $Sox2^{+}$ cells in the whole anterior SVZ. **(E)** Differences in the percentage of proliferative $Sox2^{+}$ cells in the DL-SVZ between day 3 and week 4 post-surgery. **(F-H)** Immunostains of GFAP in the DL-SVZ. **(I)** Quantification of the average length of $GFAP^{+}$ processes in anterior SVZ. **(J)** Differences in the average length of $GFAP^{+}$ processes in the DL-SVZ between day 3 and week 4 post-surgery. **(K-M)** Immunostains of DCX^{+} cells in tiers 2–3 of the DL-SVZ. **(N)** Quantification of the average density of DCX+ cells. **(O)** Differences in the average density of DCX^{+} cells in the DL-SVZ between day 3 and week 4 post-surgery. **(P-R)** Coronal sections of the SVZ showing immunostains of DCX^{+} cell clusters. **(S)** Quantification of the average number of DCX^{+} cell clusters. **(T)** Quantification of the average cluster occupancy of the SVZ. Scale bars, 50 µm (A, B, C, F, G, H, K, L, M) and 100 µm (P, Q, R). n = 4 animals per group. Data are expressed as mean ± SEM. *$p < 0.05$, **$p < 0.01$, #$p < 0.05$ control compared to severe group, \$$p < 0.05$ control compared to severe and mild groups. One-way ANOVA with Tukey's post-hoc test (D, I, N, S, T). CPB, cardiopulmonary bypass; DL-SVZ, dorsolateral-SVZ; DCX, doublecortin;

LV, lateral ventricle; SVZ, subventricular zone; V-SVZ, ventral-SVZ; GFAP, glial fibrillary acidic protein.

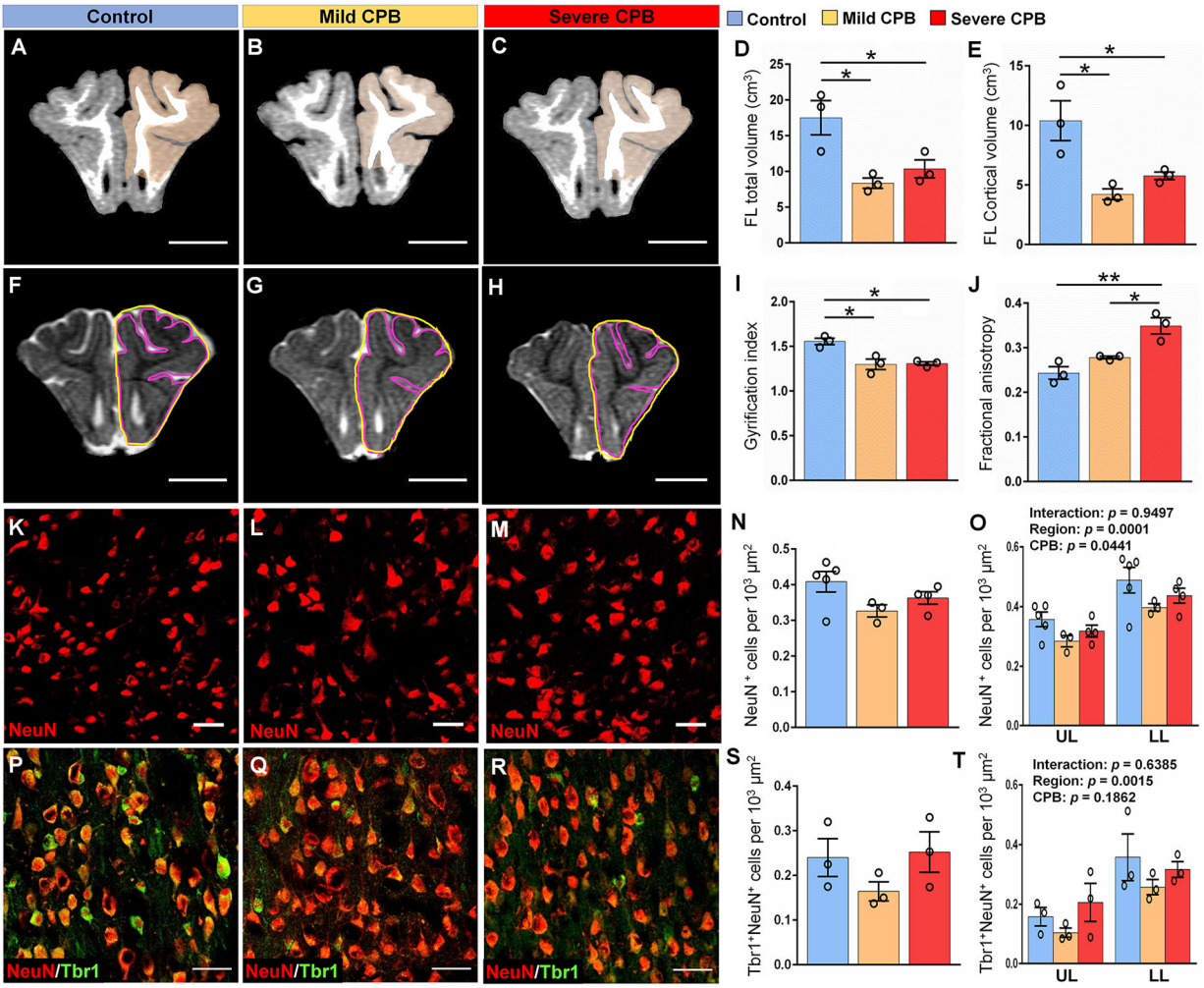

Figure 4. CPB impairs cortical development and limits cortical expansion.

(A-C) T1 MRI scans showing cortical gray matter of frontal lobe. Scale bars, 1 cm. **(D, E)** Quantification of frontal lobe total and cortical volumes. **(F-H)** Perimeter of the total pial surface (purple lines, inner) and total perimeter of the brain (yellow lines, outer) on T2 MRI scans. Scale bars, 1 cm. **(I)** Quantification of cortical folding determined by the GI expressed as a ratio of the inner versus outer perimeter traces in (F, G, H). **(J)** Quantification of fractional anisotropy in the cortex of frontal lobe. **(K-M)** Immunostains of NeuN within the lower cortical layers of the frontal lobe. Scale bars, 50 µm. **(N, O)** Quantification of the average density of $NeuN^+$ cells in the frontal lobe. **(P-R)** Immunostains of NeuN and Tbr1 within the lower cortical layers of the frontal lobe. **(S, T)** Quantification of the average density of $NeuN^+Tbr1^+$ cells in the frontal lobe. Scale bars, 50 µm. Data are expressed as mean ± SEM (n = 3–4 animals per group). *$p < 0.05$, **$p < 0.01$. One-way ANOVA with Tukey's post-hoc test (D, E, I, J, N, S) and two-way ANOVA with Tukey's post-hoc test (O, T). CPB, cardiopulmonary bypass; FL, frontal lobe; LL, lower layers; NeuN, neuronal nuclear protein; Tbr1, T-box brain 1; UL, upper layers.

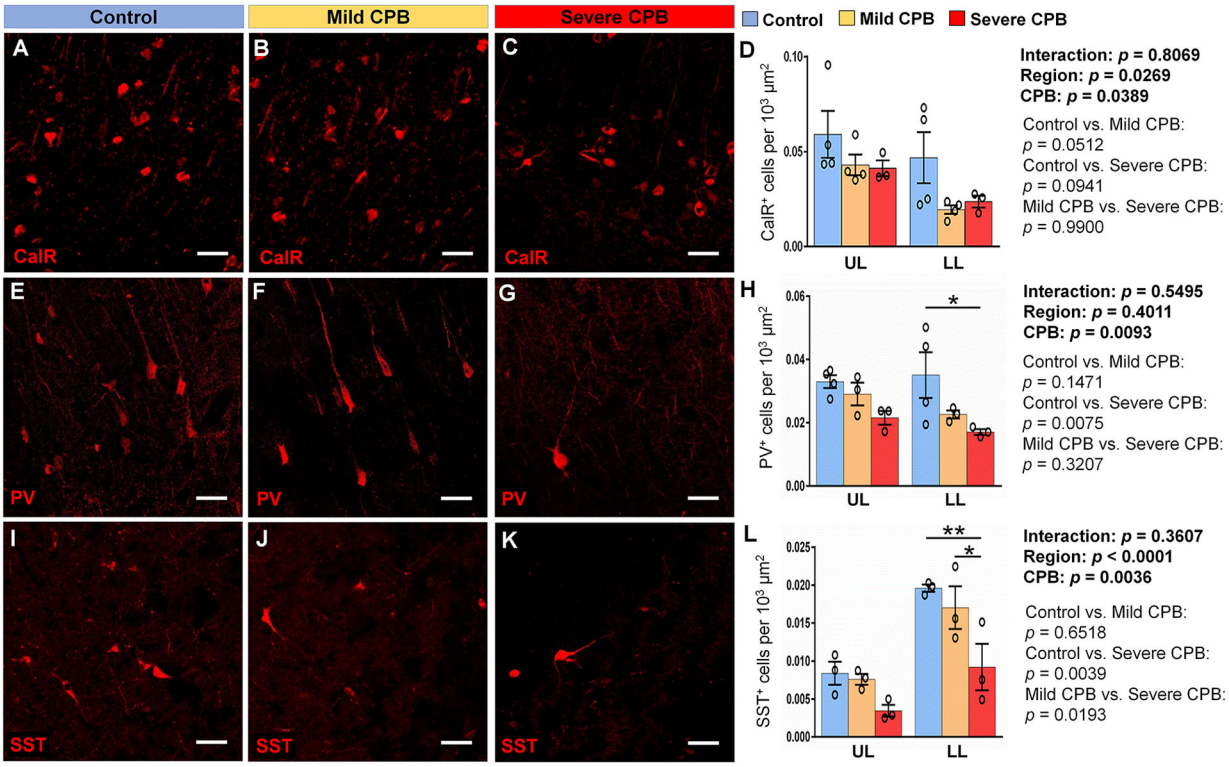

Figure 5. CPB alters interneuron cell populations in the cortex 4 weeks post-surgery.

(A-C) Immunostains of Calretinin within the lower cortical layers of the frontal lobe. **(D)** Quantification of the average density of $CalR^+$ cells. **(E-G)** Immunostains of Parvalbumin within the lower cortical layers of the frontal lobe. **(H)** Quantification of the average density of PV^+ cells. **(I-K)** Immunostains of Somatostatin within the lower cortical layers of the frontal lobe. **(L)** Quantification of the average density of SST^+ cells. Scale bars, 50 µm. Data are expressed as mean ± SEM (n = 3 to 4 animals per group). $*p < 0.05$, $**p < 0.01$, two-way ANOVA with Tukey's post-hoc test (D, H, L). CalR, calretinin; CPB, cardiopulmonary bypass; FL, frontal lobe; LL, lower layers; PV, parvalbumin; SST, somatostatin; UL, upper layers.

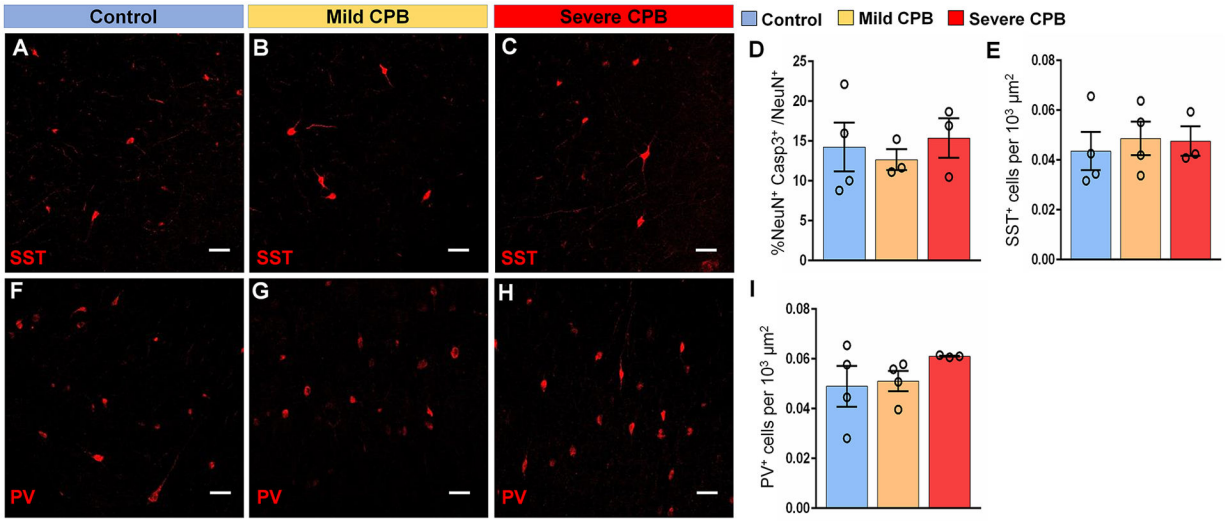

Figure 6. CPB does not alter interneuron densities in the piglet cortex 3 days after surgery.

(A-C) Immunostains of Somatostatin within the lower cortical layers of the frontal lobe. **(D)** Quantification of the average percentage of Casp3+NeuN+ within the piglet frontal lobe. **(E)** Quantification of the average density of SST+ cells. **(F-H)** Immunostains of Parvalbumin within the lower cortical layers of the frontal lobe. **(I)** Quantification of the average density of PV+ cells. n = 3 to 4 animals per group. Two-way ANOVA with Tukey's post-hoc test. Scale bars, 50 μm. Casp3, cleaved-caspase 3; NeuN, neuronal nuclear protein; PV, parvalbumin; SST, somatostatin.

Table 1.

Experimental Conditions

	Mild CPB (n=10)		Severe CPB (n=10)		
	Mean	**SD**	**Mean**	**SD**	***p* value**
Temperature (°C)					
Pre CPB	36.2	1.0	36.2	0.8	0.9999
Cooling	33.8	0.3	26.6	0.7	<0.0001 *
FF or CA	33.1	0.3	24.7	0.8	<0.0001 *
Rewarming	36.4	0.9	35.6	0.9	0.2399
3hrs	37.0	0.8	37.0	0.5	0.9999
MBP (mmHg)					
Pre CPB	83.9	19.6	80.7	15.0	0.9999
Cooling	99.7	14.1	95.5	12.9	0.9999
FF or CA	113.5	17.1	5.4	1.9	<0.0001 *
Rewarming	130.4	18.3	114.9	17.9	0.3526
3hrs	92.8	14.9	87.1	13.0	0.9999
pH					
Pre CPB	7.585	0.098	7.582	0.082	0.9999
Cooling	7.489	0.036	7.471	0.042	0.9999
Rewarming	7.546	0.033	7.458	0.034	<0.0001 *
3hrs	7.605	0.047	7.570	0.053	0.5423
$PaCO_2$ (mmHg)					
Pre CPB	32.1	6.7	33.3	6.5	0.9999
Cooling	42.8	3.1	41.8	2.2	0.9999
Rewarming	41.5	3.4	39.3	2.7	0.5092
3hrs	32.4	3.8	30.4	3.3	0.8892
Hematocrit (%)					
Pre CPB	35.5	3.6	36.9	2.3	0.9999
Cooling	34.1	1.5	33.9	1.6	0.9999
Rewarming	32.4	1.8	33.7	1.8	0.4967
3hrs	36.9	3.7	33.7	1.9	0.1200
TOI					
Pre CPB	47.7	5.3	47.2	2.4	0.9999
Cooling	58.1	3.4	64.7	5.4	0.0236 *
FF or CA	57.6	2.6	34.7	4.4	<0.0001 *
Rewarming	53.7	2.8	53.2	1.6	0.9999
3hrs	48.9	1.9	47.3	4.1	0.9999
Lactate (mmol/l)					
Pre CPB	1.4	0.4	1.4	0.4	0.9999
Cooling	2.4	0.8	2.5	0.5	0.9999
Rewarming	1.8	0.9	6.9	1.3	<0.0001 *

	Mild CPB (n=10)		Severe CPB (n=10)		
	Mean	**SD**	**Mean**	**SD**	***p* value**
3hrs	2.0	0.9	5.4	1.4	<0.0001 *
Leukocyte (10^3/μL)					
Pre CPB	5.4	1.4	6.9	1.2	0.0787
Cooling	5.7	1.8	5.3	1.4	0.9999
Rewarming	5.9	1.9	7.8	3.3	0.5948
3hrs	11.8	4.5	14.0	3.7	0.9560

CPB, cardiopulmonary bypass; MAP, mean arterial pressure; TOI, tissue oxygen index.

*Statistically significant.

Table 2.

Changes in body weight and neurological outcome

	Control (n=4–10)		Mild CPB (n=4–10)		Severe CPB (n=4–10)				Control vs.	Control vs.	Mild vs.
	Mean	SD	Mean	SD	Mean	SD	F value	*p* value	Mild	Severe	Severe
Weight (kg)											
Pre	5.1	0.7	5.0	0.8	5.0	0.4	0.072	0.930			
Day 3	5.4	0.8	5.0	0.9	4.9	0.6	1.280	0.293			
Week 4	10.5	1.7	9.1	1.8	9.1	2.2	1.161	0.338			
NDS											
Day 1	0.0	0.0	29.0	26.0	150.0	35.2	99.140	<0.0001 *	0.041 *	<0.0001 *	<0.0001 *
Day 2	0.0	0.0	0.0	0.0	89.0	52.0	29.350	<0.0001 *	0.9999	<0.0001 *	<0.0001 *
Day 3	0.0	0.0	0.0	0.0	61.5	32.5	35.820	<0.0001 *	0.9999	<0.0001 *	<0.0001 *
Day 4	0.0	0.0	0.0	0.0	26.7	35.5	3.395	0.061	0.9999	0.094	0.094
Day 5	0.0	0.0	0.0	0.0	12.5	14.8	4.310	0.033 *	0.9999	0.055	0.055
Day 6	0.0	0.0	0.0	0.0	6.7	10.3	2.500	0.116			
Day 7	0.0	0.0	0.0	0.0	0.0	0.0					

CPB, cardiopulmonary bypass; NDS, neurological deficit score.

*Statistically significant.